**Supplementary Figures, Tables, and Legends:**

Supplementary Figure 1

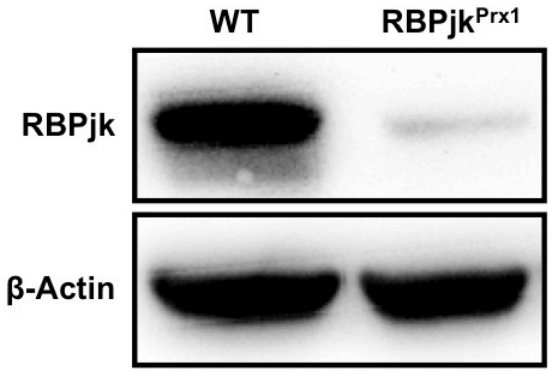


**Supplementary Figure 1.** RBPjκ is efficiently knocked down in *RBPjk*$^{Prx1}$ mutant compact bones. Western blot analyses for RBPjk in protein extracts from femurs and tibiae of wild-type (WT) controls and *RBPjk*$^{Prx1}$ mutants at 2-months of age. Results are representative of three independent experiments. N = 3 mice per genotype.

Supplementary Figure 2

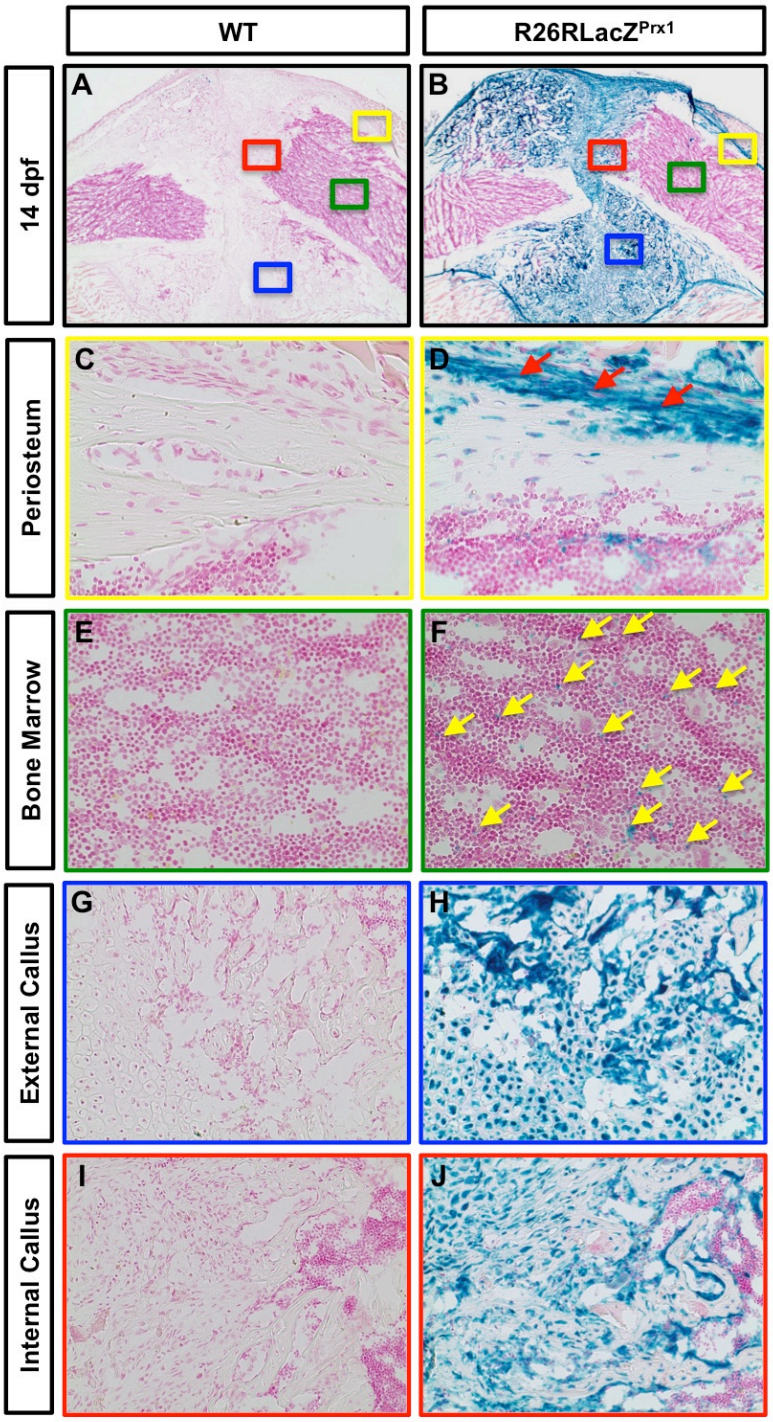


**Supplementary Figure 2.** During fracture repair, all the cells in the callus are derived from Prx1-expressing cells. X-gal staining of callus sections from Cre- WT control (A) and *R26RLacZ*$^{Prx1}$ (B) mice at 14 dpf. 20X magnification of periosteum and bone marrow revealed Prx1-expressing MSCs not only in the periosteum (red arrows) (D) but also in bone marrow (yellow arrows) (F) of *R26RLacZ*$^{Prx1}$ fractures, while no LacZ-positive cells were found in WT periosteum (C) or bone marrow (E). 20X magnification of the external and internal callus showed that all the cells in the entire callus area, including both the external callus (H) and internal callus (J), were derived from Prx1-expressing cells in *R26RLacZ*$^{Prx1}$ fractures, whereas no blue cells were detected in either the external callus (G) or the internal callus (I) of WT fractures. N = 3 mice per genotype.

Supplementary Figure 3

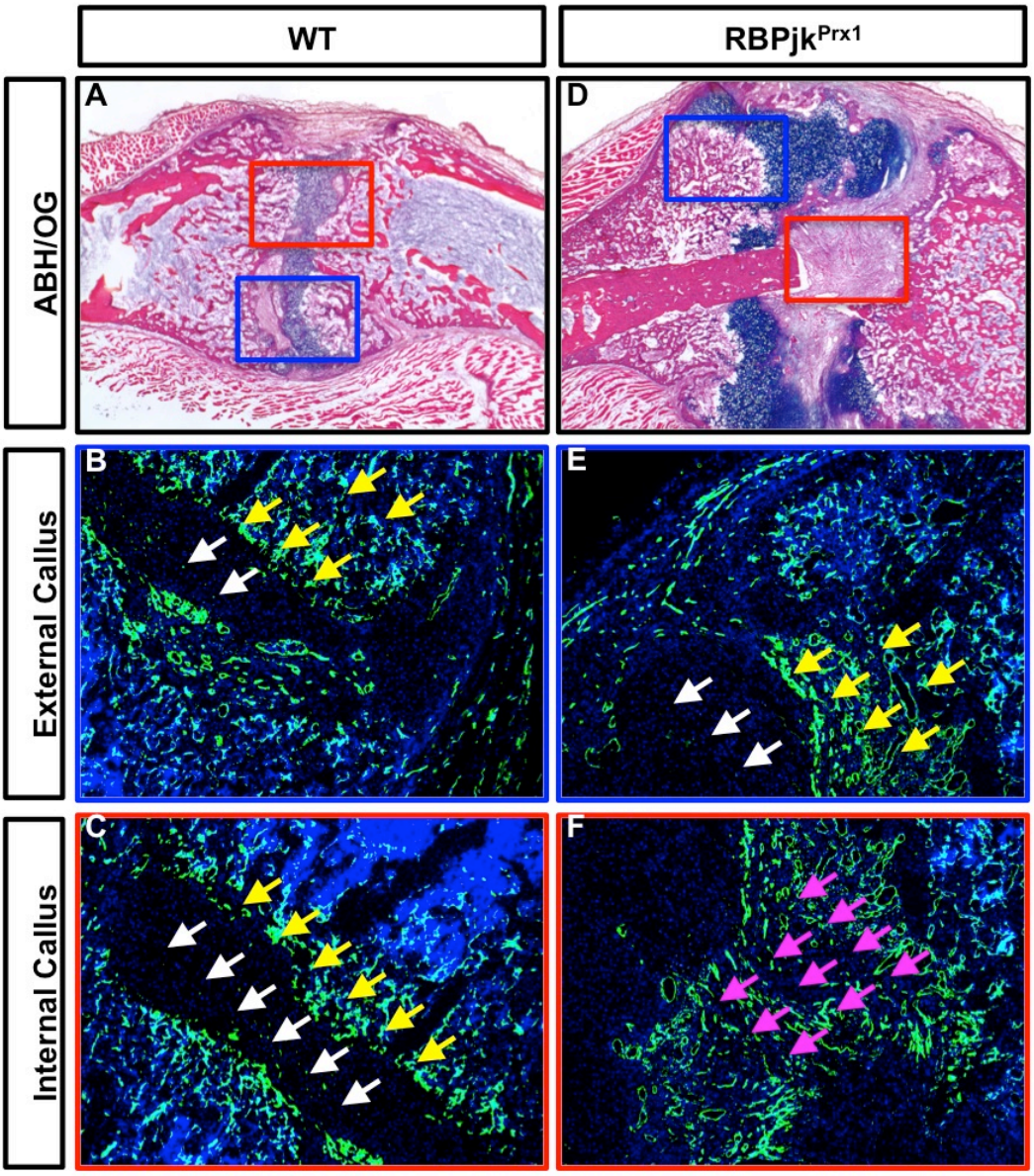


**Supplementary Figure 3.** Fracture nonunion observed in *RBPjκ*$^{Prx1}$ mutants is not attributed to a disrupted vascular network within fracture gap. ABH/OG (A, D) and IF for PECAM (B, E, C, F) on callus sections of WT and *RBPjk*$^{Prx1}$ mutants at 14 dpf. N = 5 mice per genotype. White arrow indicates no PECAM expression in the cartilaginous callus regions. Yellow arrow indicates abundant newly formed blood vessels invading the bony callus regions. Pink arrow indicates abundant PECAM expression across the fracture gap in *RBPjk*$^{Prx1}$ mutants.

Supplementary Figure 4

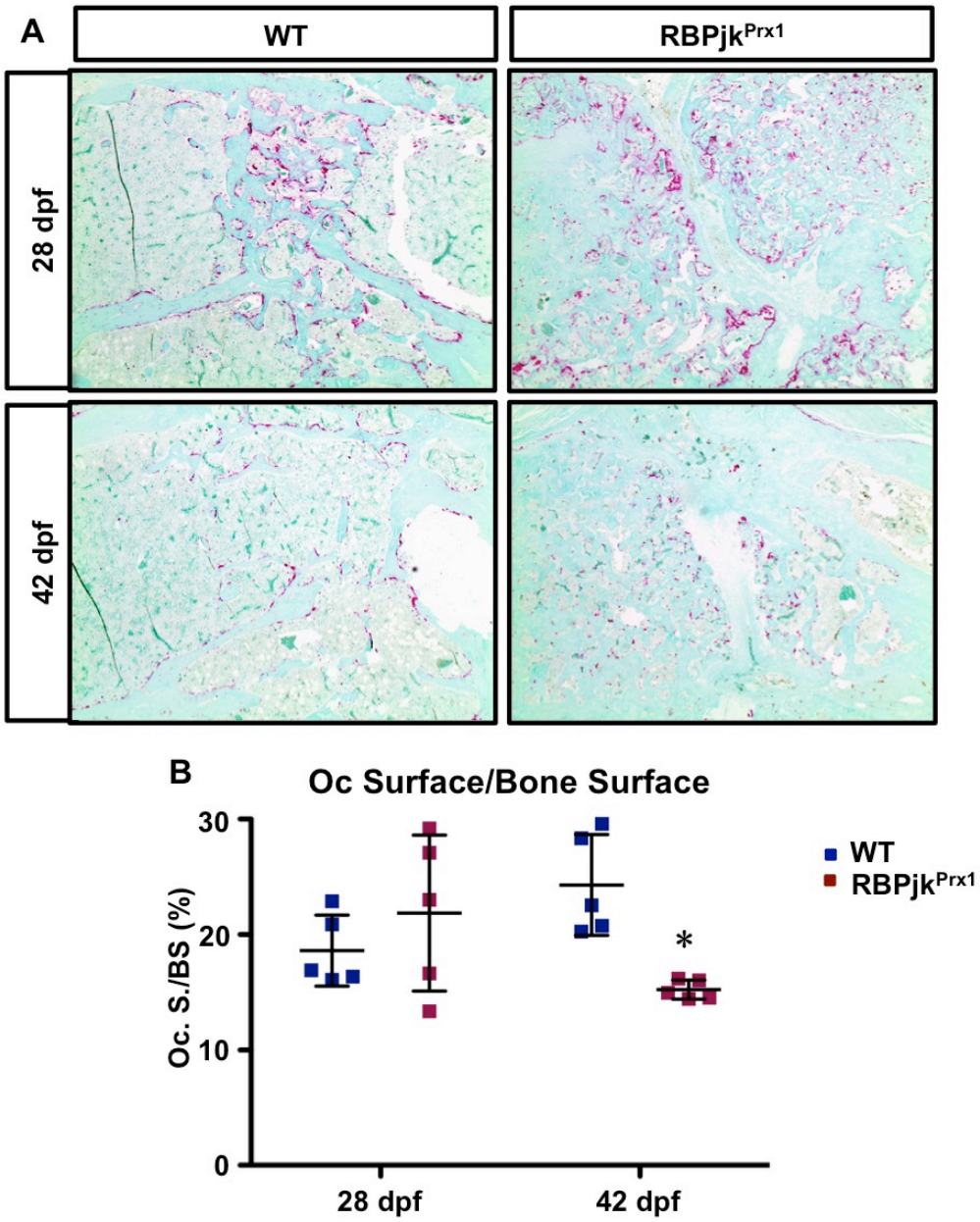


**Supplementary Figure 4.** Fracture nonunion in *RBPjk*$^{Prx1}$ mutants is not due to enhanced osteoclast numbers. (A) TRAP staining on callus sections of WT and *RBPjk*$^{Prx1}$ mutant fractures at 28 and 42 dpf. N = 5 mice per genotype per time point. (B) Histomorphometric quantifications of the osteoclast surface per bone surface (Oc. S./BS) on TRAP stained sections revealed comparable (at 28 dpf) or even significantly lower Oc. S./BS (at 42 dpf) in *RBPjk*$^{Prx1}$ mutants. N = 5 mice per genotype per time point, *, $p<0.05$ compared with WT by two-way ANOVA followed by Dunnett's post hoc test. Results are expressed as means ± SD.

Supplementary Figure 5

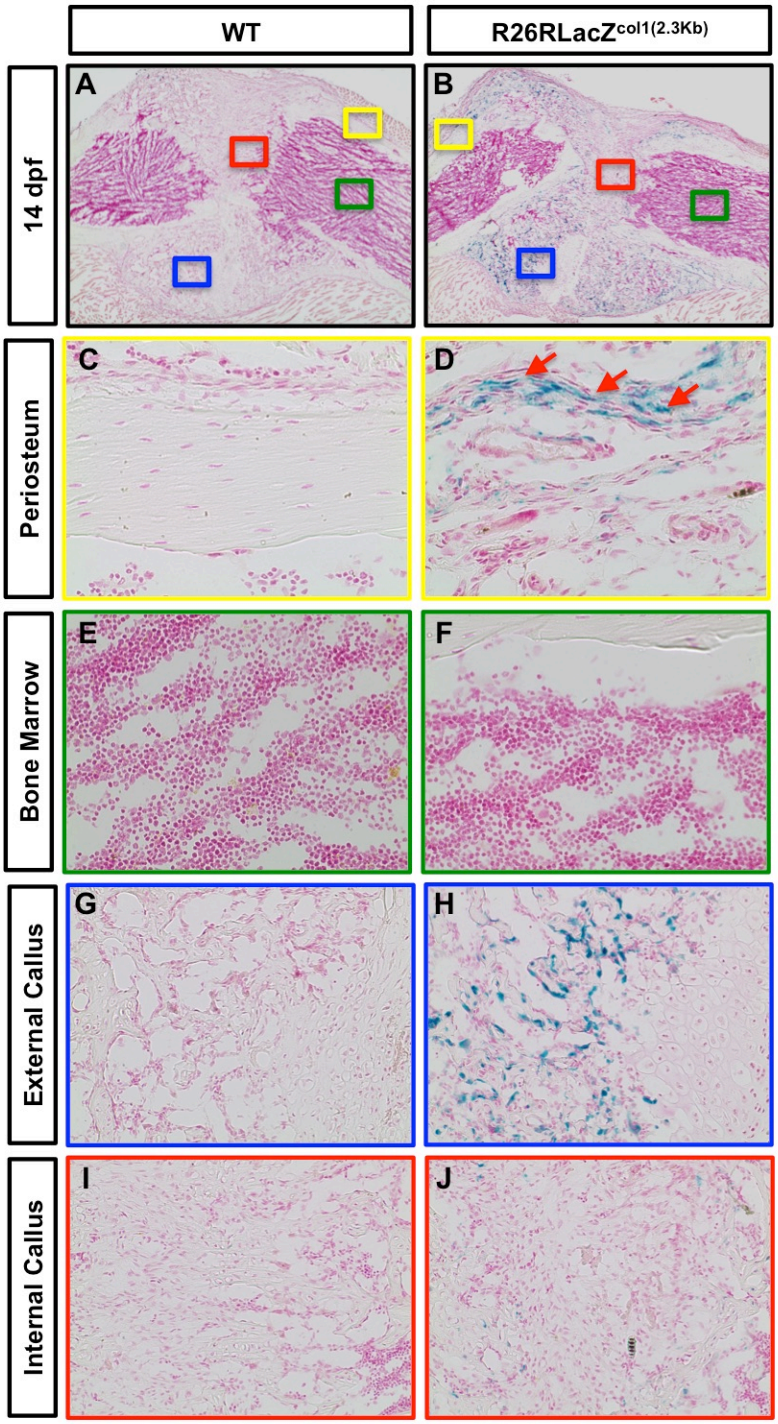


**Supplementary Figure 5.** During fracture repair, Col1 (2.3kb)-expressing cells only give rise to the cells in the hard callus regions within the external callus area. X-gal staining of callus sections from Cre- WT control (A) and *R26RLacZ*$^{Col1}$ (B) mice at 14 dpf. 20X magnification of periosteum and bone marrow revealed Col1-expressing mature osteoblasts only in the cambium layer of the periosteum (red arrows) (D) but not in bone marrow (F) of *R26RLacZ*$^{Col1}$ fractures. By contrast, no LacZ-positive cells were found in WT periosteum (C) or bone marrow (E). 20X magnification of the external and internal callus showed that the cells within hard callus regions of the external callus (H) but not internal callus (J) were derived from Col1-expressing cells in *R26RLacZ*$^{Col1}$ fractures, while no blue cells were detected in either the external callus (G) or the internal callus (I) of WT fractures. N = 3 mice per genotype.

Supplementary Figure 6

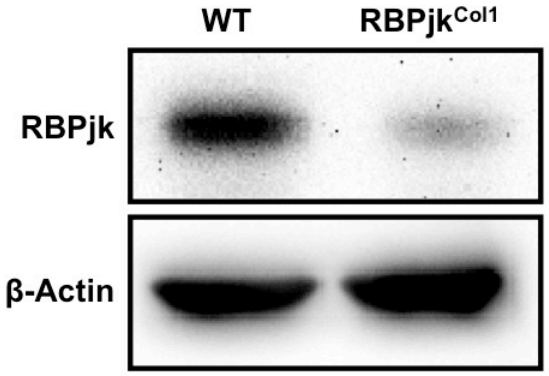


**Supplementary Figure 6.** RBPjk is efficiently knocked down in *RBPjk*$^{Col1}$ mutant compact bones. Western blot analyses for RBPjk in protein extracts from femurs and tibiae of WT controls and *RBPjk*$^{Col1}$ mutants at 2-months of age. Results are representative of three independent experiments. N = 3 mice per genotype.

Supplementary Figure 7

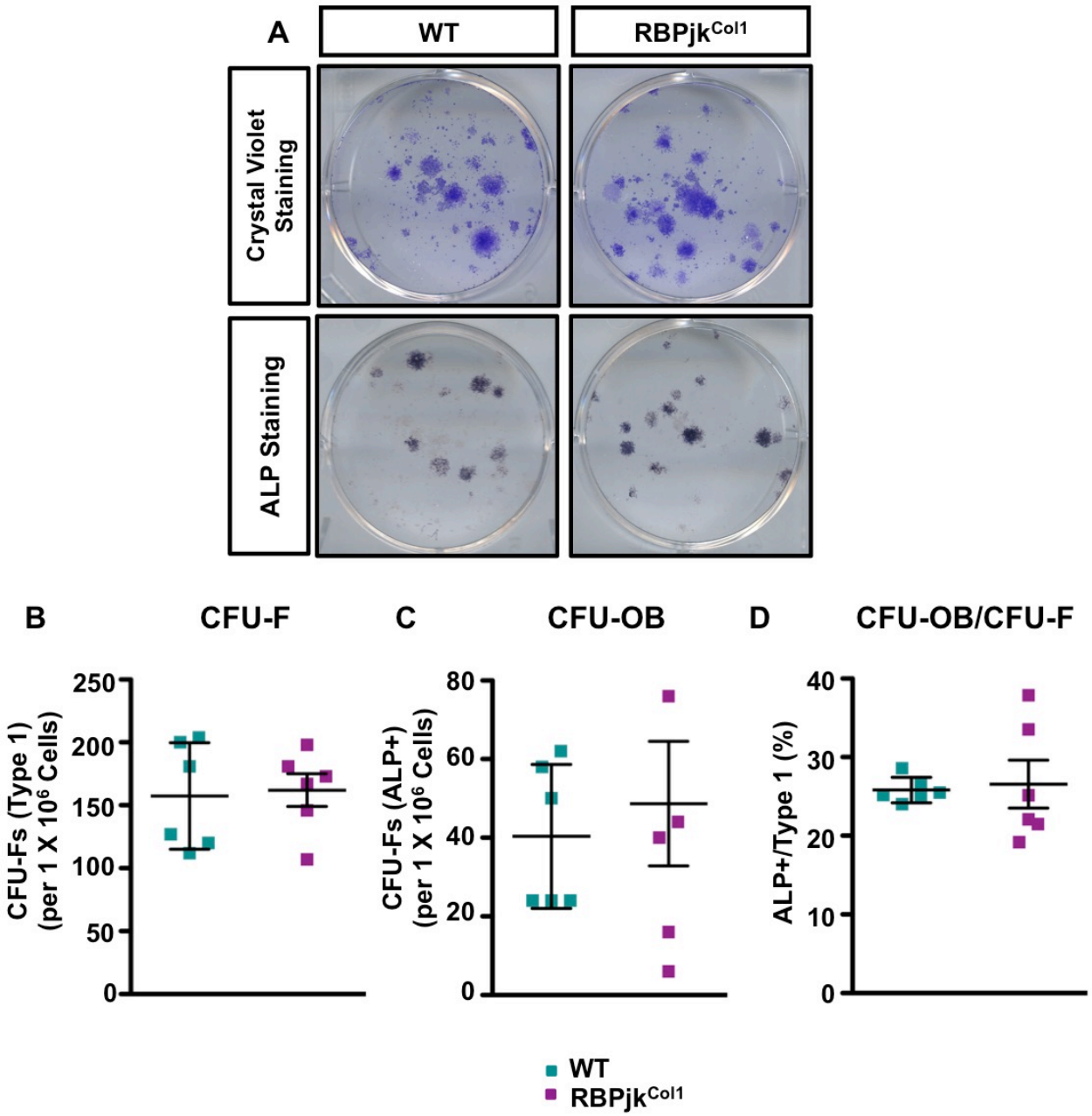


**Supplementary Figure 7.** BMSCs in *RBPjκ*$^{Col1}$ mutants are unaffected by loss of Notch signaling in mature osteoblasts. (A) CFU-F assays on bone marrow stromal cells isolated from WT and *RBPjk*$^{Col1}$ mutant fractures at 42 dpf. Representative images for crystal violet staining of CFU-Fs and ALP staining of CFU-OBs are both shown. N = 6 mice per genotype. (B-D) *RBPjk*$^{Col1}$ mutant fractures exhibited comparable type 1 colonies (CFU-Fs), ALP-positive colonies (CFU-OBs), and ratio of CFU-OB/CFU-F as compared to WT control ones. N = 6 mice per genotype. *, $p<0.05$ compared with WT by two-tailed unpaired Student's *t* test. Results are expressed as means ± SD.

Supplementary Figure 8

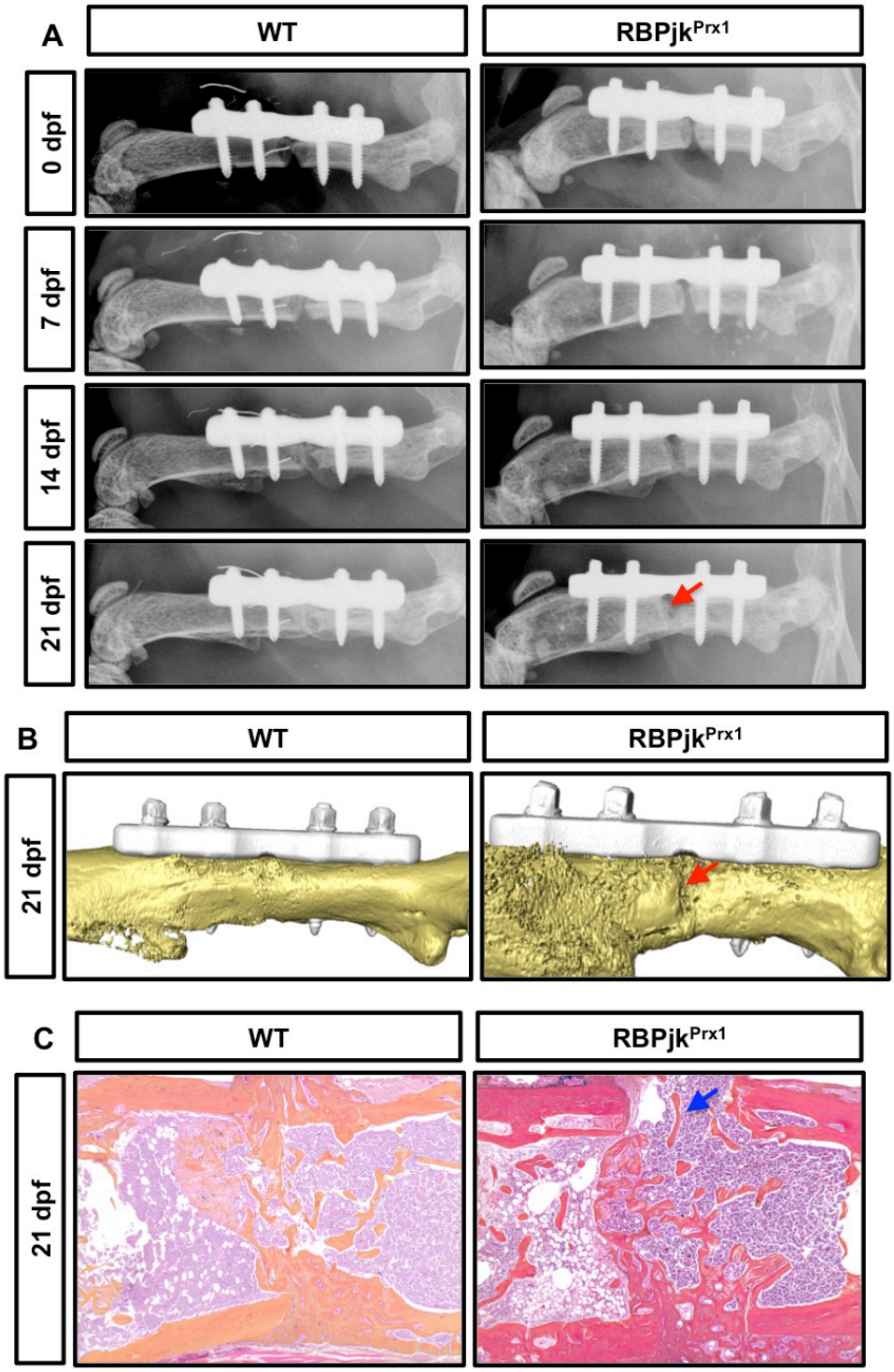


**Supplementary Figure 8.** Stabilized femur fractures (0.6-mm osteotomy) of *RBPjk*$^{Prx1}$ result in delayed unions. (A) A real-time radiographic comparison of 0.6-mm osteotomies in WT and *RBPjk*$^{Prx1}$ mutants. N = 2 mice per genotype. (B) Representative microCT images of 0.6-mm osteotomies in WT and *RBPjk*$^{Prx1}$ mutants at 21 dpf. N = 2 mice per genotype. (C) ABH/OG staining on femur fracture sections (0.66-mm osteotomy) from WT and *RBPjk*$^{Prx1}$ mutants at 21 dpf. N = 2 mice per genotype. Red arrow indicates a radiolucent area at the level of the osteotomy in both autoradiographs and microCT images of *RBPjk*$^{Prx1}$ mutants. Blue arrow indicates nearly no callus formation on one side of the cortical bone in *RBPjk*$^{Prx1}$ mutant osteotomy.

# Supplementary Table 1

| Gene Name | **Forward Sequence** | **Reverse Sequence** |
|---|---|---|
| *Hes1* | TACCCCAGCCAGTGTCAACA | TCCATGATAGGCTTTGATGACTTTC |
| *Lepr1* | GCTCAGACGTAGGATGAATAG ATG | TCACCCAGCACAATCCAAT |
| *Col1a1* | GCATGGCCAAGAAGACATCC | CCTCGGGTTTCCAGGTCTC |
| *Alp* | TGACCTTCTCTCCTCCATCC | CTTCCTGGGAGTCTCATCCT |
| *Oc* | CTTGAAGACCGCCTACAAAC | GCTGCTGTGACATCCATAC |
| *β-actin* | AGATGTGGATCAGCAAGCAG | GCGCAAGTTAGGTTTTGTCA |

**Supplementary Table 1.** Primers sequences used for real-time qPCR analyses. All sequences are reported in 5' to 3' direction.